Caian Qiu[a], Susanne M. Opalka[b], Gregory B. Olson[c], Donald L. Anton[d]
[a] Caterpillar Champaign Simulation Center, Champaign, IL, USA
[b] United Technologies Research Center, East Hartford, CT, USA
[c] Northwestern University and Questek Innovations LLC, Evanston, IL, USA
[d] Savannah River National Laboratory, Aiken, SC, USA

Thermodynamic modeling of the sodium alanates and the Na–Al–H system

The thermodynamic properties of the Al–Na and Na–Al–H systems have been assessed by combining the "calculation of phase diagram" approach with first-principles predictions. The Gibbs energies of the individual phases were thermodynamically modeled, where the model parameters were obtained from best fit optimizations to combined experimental and first-principles predicted finite temperature data. The first-principles thermodynamic predictions were based upon density functional theory ground state minimizations and direct method lattice dynamics. The predictions proved to be important adjuncts to the assessments whenever experimental measurements were lacking or not feasible. It was shown that the phase stability conditions of sodium alanates, $NaAlH_4$ and Na_3AlH_6, were well described with the present models.

Keywords: Sodium alanates; Thermodynamics; First-principles; Density functional theory; Direct method lattice dynamics

1. Introduction

The sodium alanate complex hydrides, sodium aluminum tetrahydride, $NaAlH_4$, and sodium aluminum hexahydride, Na_3AlH_6, when activated with Ti additives, have an intermediate hydrogen storage capacity and reversibility at the moderate temperatures (20–120 °C) and pressures (1–100 bar) required for fueling polymer electrolyte fuel cells [1–3]. Despite the capacity and kinetic limitations of the sodium alanates, they comprise the best performing system that has been identified so far, and they are often used as a benchmark in the evaluation of newly developed hydrogen storage materials. Thermodynamic modeling of the sodium alanates provides the means for assessing the best possible performance that can be realized under equilibrium conditions. Such modeling establishes the upper bound of the ideal hydrogen reversibility that could be attained in the absence of kinetic hindrance of the hydrogen sorption reactions. This performance limit is important for evaluating the relative effectiveness of catalysis or activation of the sodium alanate hydrogen adsorption and desorption reactions. The modeling enables prediction of thermodynamic behavior of sodium alanates and other possible co-existing phases within the Na–Al–H ternary system, over a wide range of temperatures, pressures, and compositions. It also provides the basis for fundamental understanding of the interactions of other kinetically enhancing, destabilizing, or co-reacting phases that may be combined with the Na–Al–H system.

The present work incorporated the three binary systems: Al–Na, Al–H, and Na–H, as well as that of the $NaAlH_4$ and Na_3AlH_6 ternary phases, into a thermodynamic model of the Na–Al–H ternary system. A number of experimental measurements were made on the thermodynamic properties of the alanates [1–10], of which References [4–9] were reviewed by Batzner [11]. Theoretical first-principles predictions of ground state electronic energies were also reported for one or more of the alanates [12–19]. Recently, first-principles finite temperature thermodynamic predictions for the sodium alanates have been derived from both ground state density functional theory minimized electronic energies [20–22] and the finite temperature vibrational contributions determined with the direct method lattice dynamics method [23, 24]. This theoretical advance enabled the Na–Al–H system to be thermodynamically modeled by application of the "calculation of phase diagram" (CALPHAD) approach to a combination of measured and first-principles predicted finite temperature thermodynamic values. This integrated approach yielded a more robust thermodynamic description of the Na–Al–H system, capable of extending well beyond the temperature and pressure conditions that have been examined experimentally.

2. Experimental

2.1. Binary experimental descriptions

The first step in the assessment of the Na–Al–H system was to examine the thermodynamic models of the lower order Al–Na, Al–H, and Na–H binary systems. The binary Al–H and Na–H systems were already reported by the present authors [25, 26] and will be summarized briefly in the following paragraphs. The thermodynamic description of the Al–Na system has not been reported in the literature, and was developed as described in the present work.

A part of the Al–H phase diagram at 1 atm determined from the previous thermodynamic modeling [25], is shown in Fig. 1. It has a eutectic reaction at 660 °C, very close to the melting temperature of Al: liquid $\rightarrow$ Al(fcc) + H_2(gas), where fcc is the face-centered cubic $Fm\bar{3}m$ structure. The hydrogen solubility in both liquid and fcc Al is very small (0.0018 and 0.0001 at.%, respectively), according to the model prediction at the eutectic temperature at 1 atm. The

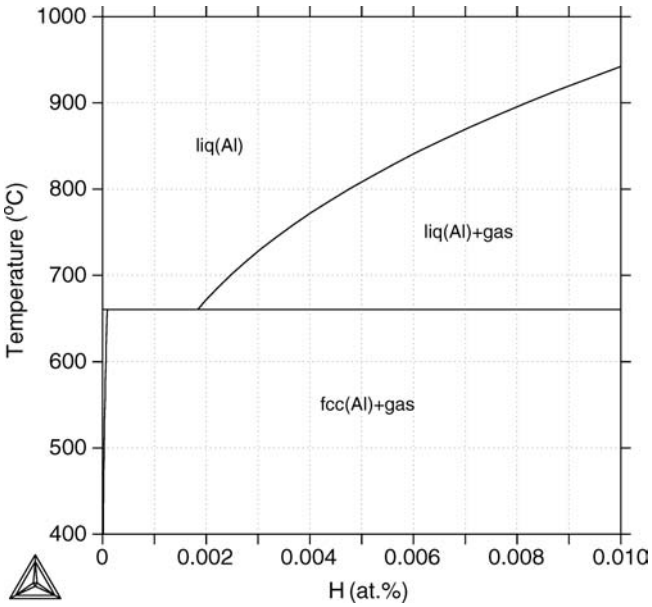

Fig. 1. A part of the Al–H phase diagram calculated at 1 atm [25].

metastable compound alane, AlH_3, is not shown in Fig. 1 because it becomes stable only at high pressures.

The fcc NaH phase is the only stable hydride in the Na–H system [26], and it decomposes to liquid Na and H_2 at 426 °C, as shown in Fig. 2. No melting of NaH would occur during heating under ambient pressure. The hydrogen solubility in solid Na is negligible (10^{-8} at.%), while the solubility in liquid Na is also small (10^{-5} at.%) at the melting temperature of Na (98 °C) at 1 atm.

The experimental data of the Al–Na system were reviewed by Murray [27]. The Al–Na phase diagram exhibits a monotectic reaction: liquid → Al(fcc) + Na(liquid), around the melting temperature of Al, and a non-symmetric miscibility gap above the monotectic reaction, as shown in Fig. 3a and b, respectively. The liquidus and monotectic reaction temperatures were measured with high accuracy by Fink [28], but their measurement of the pure Al melting temperature was about 0.2 °C lower than the model prediction. As a consequence, their data was calibrated by adding 0.2 °C and served as target values in the optimization of model parameters. Sodium solubility in liquid Al has been investigated experimentally several times [28–30], but the data from different investigators showed considerable scatter, as reviewed by Murray [27]. These solubility data ranged from 0.1 to 0.3 at.% within the temperature range from 650 to 800 °C. Recent activity measurements by Hansen [31] determined the sodium solubility to be 1.25 at.% in liquid Al at 750 °C, indicating a further discrepancy with the previous data. The activity data from Hansen [31] also dif-

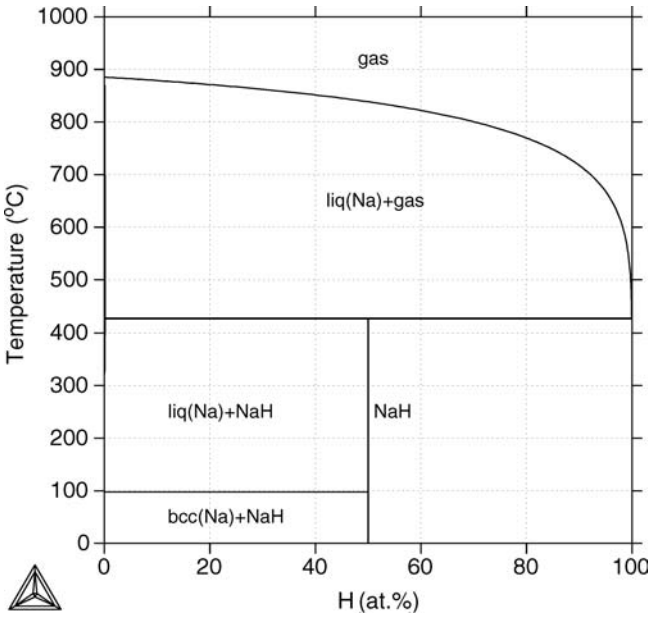

Fig. 2. The Na–H diagram calculated at 1 atm [26].

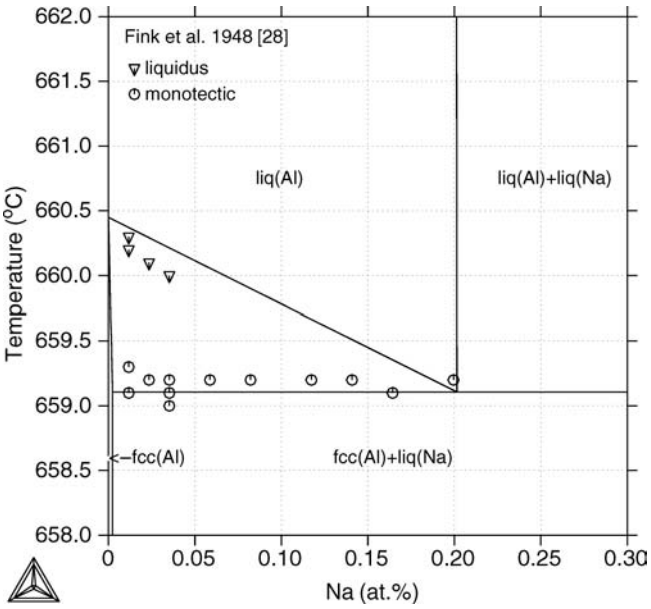

(a)

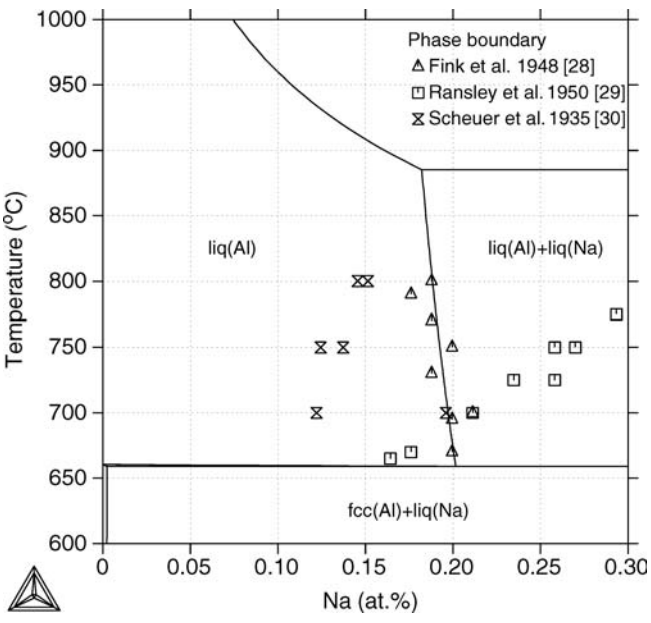

(b)

Fig. 3. The Al–Na diagram calculated according to the present modeling in comparison with experimental data. (a) A monotectic reaction close to the melting of Al, where the experimental data were calibrated by adding 0.2 °C. (b) A miscibility gap between Al(liquid) and Na(liquid).

fered significantly from the others [32, 33]. Within the scope of the present work on the modeling of sodium alanates, it was not attempted to justify the solubility and activity data. Instead, a preliminary evaluation of the Al–Na system was made by fitting the experimental monotectic reaction and solubility data of Reference [28].

The binary Al–Na liquid and solid solution phases (fcc and body-centered cubic $Im\bar{3}m$ [bcc], respectively) were thermodynamically modeled with a substitutional solution model. To model the non-symmetric miscibility, a subregular solution model was necessary for the liquid phase. On the other hand, a regular solution model was efficient for the fcc and bcc structures. All the model parameters obtained from the optimization are listed in the Appendix. The calculated Al–Na diagram is shown in Fig. 3a and b in comparison with the experimental data. From Fig. 3a it is seen that the model calculations are in very good agreement with the experimental liquidus and monotectic temperature, which were calibrated by adding 0.2 °C. Figure 3b shows that the present calculations are consistent with the solubility data from Reference [28], but are different from the others [29, 30].

2.2. Ternary Na–Al–H experimental data

A brief review of the Na–Al–H system was presented by Batzner [11]. Only the two ternary compounds, $NaAlH_4$ and Na_3AlH_6, have been observed in the Na–Al–H system. Solid $NaAlH_4$ has a tetragonal $I4_1/a$ structure and its melting was observed around 181 °C with an enthalpy of 3.871 kJ (mole atom)$^{-1}$ and entropy of 8.525 J (mole atom)$^{-1}$K^{-1} [5]. Na_3AlH_6 exists in two modifications, and the transformation from the monoclinic $P2_1/c$ α-Na_3AlH_6 to the cubic $Fm\bar{3}m$ β-Na_3AlH_6 was reported to have an enthalpy of 0.360 kJ (mole atom)$^{-1}$ at 252 °C [5]. A thermal effect was detected at 292 °C when heating β-Na_3AlH_6, which was possibly related to its melting [5].

The thermodynamic properties of the alanates have been reported based on experimental measurements. The heat capacities of $NaAlH_4$ and α-Na_3AlH_6 were measured by Bonnetot [6] in the temperature range from 0 to 300 K. The standard enthalpy of formation of $NaAlH_4$ was determined to be −18.828 kJ (mole atom)$^{-1}$ by measuring the heat of reaction with HCl [7], which agrees well with −19.50 kJ (mole atom)$^{-1}$ reported by Claudy [8] from the calorimetric measurement of the heat of the exchange reaction between $NaAlH_4$ and LiBr(solution). There are no direct data available for the enthalpy of formation of α-Na_3AlH_6. However, the enthalpy for the decomposition reaction: α-$Na_3AlH_6 \rightarrow 3NaH + Al + 1.5H_2$, was reported from differential scanning calorimetrical measurements [5]. The dissociation pressures of liquid $NaAlH_4$ and solid α-Na_3AlH_6 were measured by Dymova [9]. More studies have been carried out to investigate their hydrogenation/dehydrogenation processes with various catalysts, as reviewed by Bogdanovic [34]. Experimental data of the dissociation pressures for solid $NaAlH_4$ and α-Na_3AlH_6 doped with $TiCl_3$ [1–3] can be used as a guideline to assess their thermodynamic properties. Recently, differential scanning calorimetry and thermogravimetric measurements have quantified enthalpies for the various sodium alanate transitions determined while heating with a range of rates and hydrogen overpressures [10].

2.3. First-principles Na–Al–H thermodynamic property predictions

The enthalpies of formation or decomposition of $NaAlH_4$ and Na_3AlH_6 were predicted at finite temperatures based on the first-principles direct method lattice dynamics and were found to be consistent with the experimental data. Two methodologies were coupled for the first-principles prediction of thermodynamic properties of the solid-state phases in the Na–Al–H system. These methodologies were detailed in our preceding paper on the Na–H binary system [26] and will only be briefly summarized in the present discussion. The first methodology was a full structure minimization at the ground state (0 K) using the density functional theory (DFT) implemented in the Vienna Ab initio Simulation Package (VASP) with plane wave basis sets [21, 22]. The second methodology generated finite temperature thermodynamic predictions of the minimized structure using the direct method lattice dynamics approach of Parlinski, implemented in the Materials Design Phonon direct method module interfaced with the VASP code [23, 24] (herein referred to as the "Phonon direct method"). The solid-state phases atomically modeled in the Na–Al–H system included: the $I4_1/a$ $NaAlH_4$, the $P2_1/c$ α-Na_3AlH_6, and the fcc NaH line compounds, and the fcc Al and bcc Na elemental phases. The cubic $Fm\bar{3}m$ or the orthorhombic Immm β-Na_3AlH_6 isomorphs were not considered in this study.

For the first methodology, VASP minimizations employed the generalized gradient approximation (GGA) of Perdew and Wang [35], and the valence electrons were explicitly represented with projector augmented wave (PAW) potentials [36], using the hard Na_sv potential for the Na $2s^2 2p^6 3s^1$ valence configuration, and the regular potentials for the Al $3s^2 3p^1$ and H $1s^1$ valence configurations. The plane wave cut-off energy of 780 eV and the Gaussian smearing with an energy broadening of 0.2 eV was used. Odd-sized k-point meshes were created by a Monkhorst–Pack scheme for minimization of the primitive cells [37], using a 7 7 7 k-mesh for Al, a 5 5 5 k-mesh for $NaAlH_4$, and a 7 7 7 k-mesh for α-Na_3AlH_6. The convergence criterion for the electronic self-consistent calculations was 0.01 meV (unit cell)$^{-1}$. The ground state (0 K) structure was determined by minimizing the Hellman–Feynman forces with the conjugate gradient algorithm, until all of the ionic forces were less than 0.05 eV Å^{-1}. The quasi-harmonic and longitudinal and transverse optical (LO/TO) phonon mode splitting approximations were not applied. These approximations would have required significantly greater computational resources than would have been worthwhile in terms of increases in accuracy.

For the second methodology, the Phonon direct method was employed to predict the lattice dynamics of the VASP minimized Al, $NaAlH_4$, and α-Na_3AlH_6 structures, using the harmonic approximation. Atom displacements were made on a $2\times2\times2$ supercell for Al (32 atoms), and on $2\times2\times1$ supercells of $NaAlH_4$ (96 atoms) and of α-Na_3AlH_6 (80 atoms), where the supercells were constructed from the respective conventional cells. The corresponding Phonon direct method predictions for the Na and NaH phases were detailed in the preceding paper on the Na–H binary system [26]. A 0.1 strength of condition factor was applied for translational invariance. The finite tem-

perature Gibbs free energy $G(T)$ values referred to the stable element reference (GHSER) were determined from the analysis of the lattice dynamics following the methodology described in the preceding Na–H paper [26].

2.4. Thermodynamic modeling and evaluation of the Na–Al–H system

There are four types of phases in the ternary Na–Al–H system: liquid, solid solution (bcc and fcc), stoichiometric line compounds, and gas. They were treated with different thermodynamic models, as listed in Table 1. The models for the liquid, solid solution (bcc and fcc), and gas were extended from those used in the binary systems [25, 26]. No ternary interaction parameters were introduced due to the lack of relevant information. The gaseous phase was approximated as an ideal gas in the present modeling, as treated in the previous work [25, 26]. It includes the gaseous species Al, AlH, AlH_2, AlH_3, Al_2, H, H_2, Na, Na_2, and NaH, with H_2 being the dominant one in most cases. Their descriptions were taken from the Scientific Group Thermodata Europe (SGTE) database [38] which is based on the JANAF Tables [39].

All stoichiometric line compounds were described with sublattice models based on their crystal structure and atomic arrangement in the lattice. The Gibbs energies of AlH_3 and NaH were evaluated in previous works [25, 26]. $NaAlH_4$, α-Na_3AlH_6, and β-Na_3AlH_6 were modeled with three sublattices, providing the capability to describe the possible dissolution of other elements such as Li substituting for Na, and Ti substituting for Al. With thermodynamic modeling, the Gibbs energy of a compound is often expressed as a function of temperature with a polynomial form. Such a polynomial is quite acceptable in many cases and has often been used in the CALPHAD approach. However, the polynomial cannot model heat capacity well at very low temperatures. On the other hand, Einstein's model based on harmonic lattice vibrations can describe heat capacity reasonably well under normal conditions. In the present case, heat capacity of $NaAlH_4$ and α-Na_3AlH_6 are available from experiments in the temperature range from 0 K to 300 K and also from the Phonon direct method prediction within the range from 0 K to 2000 K. To model heat capacity over the whole temperature range, it is necessary to combine Einstein's model and the polynomial model, as shown in the previous work [26]. Thus, the Gibbs energy per one mole of formula of $NaAlH_4$ or α-Na_3AlH_6 is given by

$$G_m^o = E_o + 3RT\ln[\exp(0.5\theta_E/T) - \exp(-0.5\theta_E/T)] - 0.5A_oT^2$$

for $0\ \mathrm{K} < T < 298.15\ \mathrm{K}$ (1a)

$$G_m^\circ = a + bT + cT\ln T + dT^2 + eT^3 + \frac{f}{T}$$

for $298.15\ \mathrm{K} < T < 2000\ \mathrm{K}$ (1b)

where θ_E in Eq. (1a) is the Einstein temperature. The coefficients E_o and A_o in Eq. (1a) and $a, b, c, \ldots$ in Eq. (1b) are constants. The enthalpy, entropy, and heat capacity can be derived from the above equations using standard thermodynamic relations. As an example, heat capacity C_P is given below:

$$C_P = 3R\left[\frac{\theta_E}{T}\right]^2 \frac{\exp(\theta_E/T)}{[\exp(\theta_E/T)-1]^2} + A_oT$$

for $0\ \mathrm{K} < T < 298.15\ \mathrm{K}$ (2a)

$$C_P = -c - 2dT - 6eT^2 - 2\frac{f}{T^2}$$

for $298.15\ \mathrm{K} < T < 2000\ \mathrm{K}$ (2b)

The first term in Eq. (2a) describes harmonic lattice vibrations based on Einstein's model [40], and the second term is used to account for electronic excitation and low-order anharmonic vibrations. The polynomial in Eq. (2b) is based on the well-known Meyer–Kelley expression [41]. Similarly, Eqs. (1a) and (1b) were also applied to β-Na_3AlH_6 by assuming that the heat capacity was the same as α-Na_3AlH_6.

The properties of $NaAlH_4$ and α-Na_3AlH_6 were assessed using the above models. The first step was to evaluate the coefficients θ_E and A_o in Eq. (2a) and c, d, e, f in Eq. (2b) for the two compounds based on the experimental and Phonon direct method predicted heat capacities. During the course of this work, it was found necessary to use 6RT instead of 3RT in Eq. (1a) when applying it to α-Na_3AlH_6 because this compound has more atoms. To ensure a smooth variation of C_P around 298.15 K, a condition was used in the optimization that the difference of Eq. (2a) and Eq. (2b) at 298.15 K was set to be less than 0.1 J mol^{-1} K^{-1}.

The next step was to evaluate E_o in Eq. (1a) and a, b in Eq. (1b) by best fitting to the experimental data and first-principles calculations. The former includes transformation temperatures, transformation enthalpies, and dissociation pressure. Due to the lack of dissociation pressure data for solid $NaAlH_4$, similar data [1–3] obtained from $NaAlH_4$ with a $TiCl_3$ catalyst were used as a guideline in the evaluation. As for α-Na_3AlH_6, the selected dissociation data [1, 3] obtained with a $TiCl_3$ catalyst compared well with those by Dymova [9]. However, the data by Bogdanovic [2] showed a significant deviation from the others, and hence were not used in the evaluation of the model parameters. All the parameter evaluations were carried out through optimization using the Thermo-Calc PARROT program [42]. The various types of input data were treated simultaneously, and the parameters were optimized by searching for the best fit to selected data.

Table 1. Phases and compounds formed in the Na–Al–H system and their corresponding thermodynamic models. Va denotes vacancy.

Phase	Thermodynamic model	Formula
Liquid	substitutional solution	(Al, Na, H)
bcc	interstitial solution	$(Al, Na)_1(H, Va)_3$
fcc	interstitial solution	$(Al, Na)_1(H,Va)_1$
NaH	2-sublattice model	$(Na)_1(H)_1$
AlH_3	2-sublattice model	$(Al)_1(H)_3$
$NaAlH_4$	3-sublattice model	$(Na)_1(Al)_1(H)_4$
α-Na_3AlH_6	3-sublattice model	$(Na)_3(Al)_1(H)_6$
β-Na_3AlH_6	3-sublattice model	$(Na)_3(Al)_1(H)_6$
Gas	ideal gas	

3. Results and discussion

3.1. First-principles predicted properties

The ground state sodium alanate structure lattice parameters determined in this study are compared to experimental results [43–46] in Table 2. The agreement with experiment

Table 2. Comparison of predicted (this study) and experimental lattice parameters for the sodium alanate phases. Reference [50] should be consulted for a review of lattice parameters determined by other theoretical calculations. The abbreviation PXD is used for powder X-ray diffraction and PND for powder neutron diffraction.

Na–Al–H Phase (Space Group)	Minimized Lattice Parameter(s) (Å)			β angle (°C)	Analyses/*T* (K)
	a	*b*	*c*		
Al ($Fm\bar{3}m$)					
Calculated	4.0458	4.0458	4.0458	–	–/0
Experimental [43]	4.0494	4.0494	4.0494	–	PXD/298
$NaAlH_4$ ($I4_1/a$)					
Calculated	5.0004	5.0004	11.1141	–	–/0
Experimental [44]	5.0265	5.0265	11.3706	–	PXD/298
Experimental [45]	4.9802	4.9802	11.1482	–	PND/8
α-Na_3AlH_6 ($P2_1/n$)					
Calculated	5.3565	5.5443	7.7173	89.91	–/0
Experimental [44]	5.4536	5.547	7.811	89.83	PXD/453
Experimental [46]	5.408	5.538	7.757	89.83	PXD/295

is acceptable, considering the difference in experimental and prediction temperatures and the absence of quasi-harmonic corrections. These structural results are in general good agreement with those reported by other sodium alanate DFT studies [12–19, 47–50], of which many of the $NaAlH_4$ results have been recently reviewed by Frankcombe [50]. The electronic energies and heats of formation of the minimized structures computed in this study are listed in Table 3. The electronic heats of formation can be compared to the other reported theoretical values. Wolverton [13] reported $-64\ kJ\ mol^{-1}$ for $NaAlH_4$, $-150\ kJ\ mol^{-1}$ for α-Na_3AlH_6, and $-43\ kJ\ mol^{-1}$ for NaH. Ke [15] reported a heat of formation of $-46.3\ kJ\ mol^{-1}$ for NaH. The Phonon direct method dispersions for the $NaAlH_4$, and α-Na_3AlH_6 phases are shown in Fig. 4a and b. If LO/TO corrections were applied, the resulting $NaAlH_4$ Phonon direct method dispersion would be similar to those shown by Ke [15].

3.2. Thermodynamic assessment

The thermodynamic description of the Na–Al–H system is given in the Appendix, where the model parameters marked with an asterisk were evaluated in the present work. The description can be used to make thermodynamic calculations under different conditions. The calculated heat capacities of $NaAlH_4$ and α-Na_3AlH_6 are presented in Fig. 5a and b in comparison with experimental data and the Phonon direct method predictions. From these comparisons there is a satisfactory agreement between the predictions and the experimental data, indicating the validity of this theoretical methodology. The present thermodynamic model combining Einstein's expression at low temperatures and the polynomial expression at high temperatures can account for all the data within the whole temperature range from 0 to 2000 K.

Table 3. Predicted parameters for H_2 gas, and the Na, Al, $NaAlH_4$, α-Na_3AlH_6, and NaH solid phases, based on the first-principles calculations. The parameters for the H_2 gas, the Na and NaH solid phases are from the preceding paper on the Na–H binary system [26].

Phase (Space Group)	Minimized Electronic E $E(0)_{elect}$ ($kJ\ mol^{-1}$)	Electronic Heat of Formation $\Delta H_{elect\ form}$ (0 K) ($kJ\ mol^{-1}$)	Zero Point Energy (*ZPE*) ($kJ\ mol^{-1}$)	Enthalpy Difference ($H_{298} - H_0$) ($kJ\ mol^{-1}$)
H_2 (gas)	−652.42	–	26.33	8.46
Na ($Im\bar{3}m$)	−127.90	–	1.44	6.46
Al ($Fm\bar{3}m$)	−356.01	–	3.65	4.54
$NaAlH_4$ ($I4_1/a$)	−1894.03	−105.29	77.33	13.66
α-Na_3AlH_6 ($P2_1/c$)	−2906.74	−209.78	111.40	24.63
NaH ($Fm\bar{3}m$)	−498.80	−44.68	15.04	6.12

As observed in experiments [6], $NaAlH_4$ decomposes in two steps

$$NaAlH_4 \rightarrow 1/3\alpha\text{-}Na_3AlH_6 + 2/3Al + H_2 \quad (3a)$$

$$\alpha\text{-}Na_3AlH_6 \rightarrow 3NaH + Al + 1.5H_2 \quad (3b)$$

The dissociation pressure for each reaction can be calculated from the following equations

$$P_{H2} = \exp(-\Delta G_1/RT) = \exp(-\Delta H_1/RT + (S_1/R)$$

[for reaction Eq. (3a)] (4a)

$$P_{H2} = \exp(-\Delta G_2/1.5RT) = \exp(-\Delta H_2/1.5RT + (S_2/1.5R)$$

[for reaction Eq. (3b)] (4b)

where ΔG_1 and ΔG_2 are the Gibbs energies of reaction Eqs. (3a) and (3b), respectively. Within a certain temperature range, the dissociation enthalpy ΔH and entropy ΔS are almost constant. A linear relation is then expected between dissociation pressure and reciprocal temperature in an Arrhenius plot, i. e. $\ln(P_{H2})$ vs. $1/T$, as shown in Fig. 6 in comparison with experimental data. It can be seen that the calculations are in very good agreement with most experimental data [1, 3, 9], except those from Bogdanovic [2]. It is also noted that the present calculations are in line with the Phonon direct method predictions. According to the present calculations, α-$NaAlH_6$ transforms to β-$NaAlH_6$ at 252 °C with an enthalpy of 0.35 kJ (mole atom)$^{-1}$, compared to experimental data of 0.36 kJ (mole atom)$^{-1}$. However, the present modeling was not parameterized to predict the melting of $NaAlH_4$ at 181 °C or that of β-Na_3AlH_6 at 292 °C.

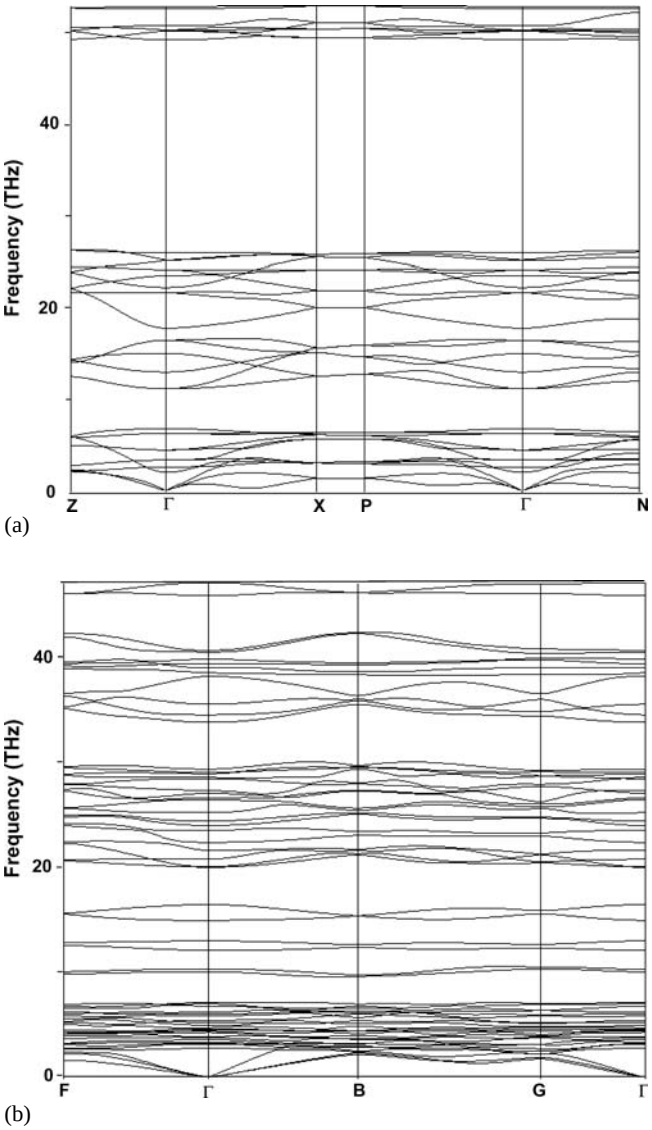

Fig. 4. The predicted phonon dispersions along the high symmetry directions in the Brillouin zones of (a) $NaAlH_4$, and (b) α-Na_3AlH_6 determined using P1 representation.

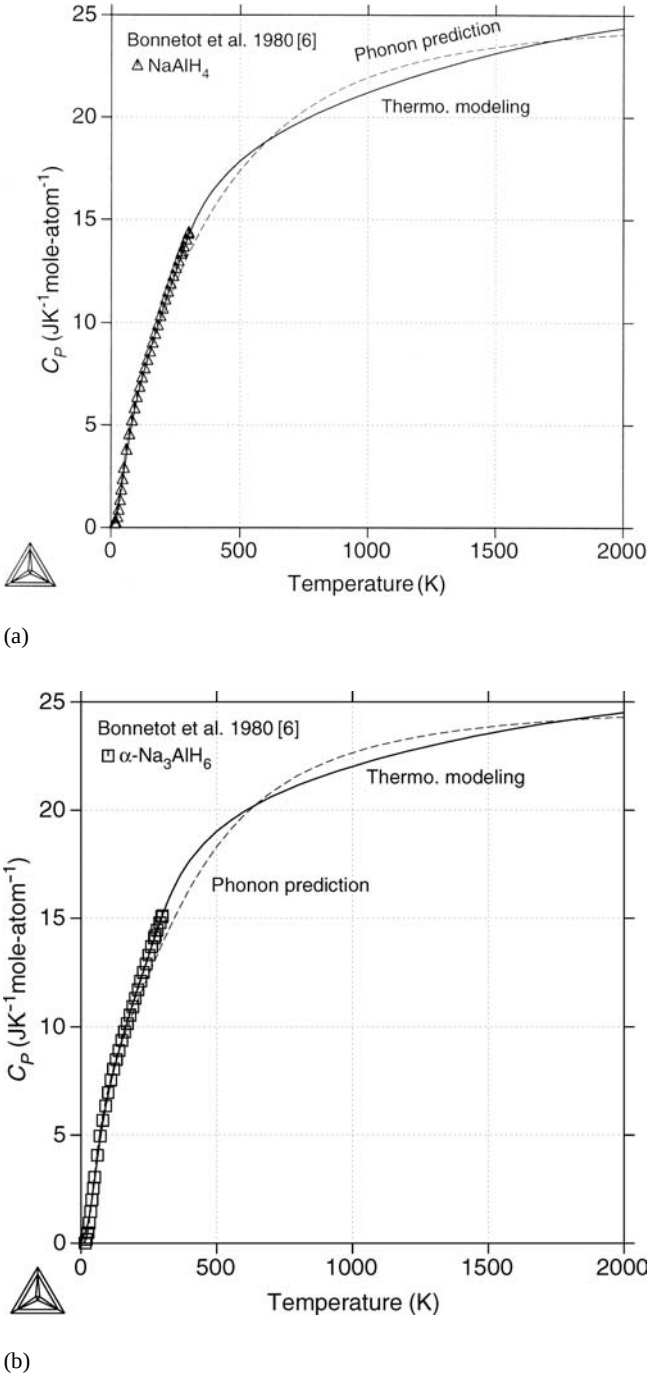

Fig. 5. Calculated heat capacity of (a) $NaAlH_4$ and (b) α-Na_3AlH_6 in comparison with experimental data and Phonon direct method predictions.

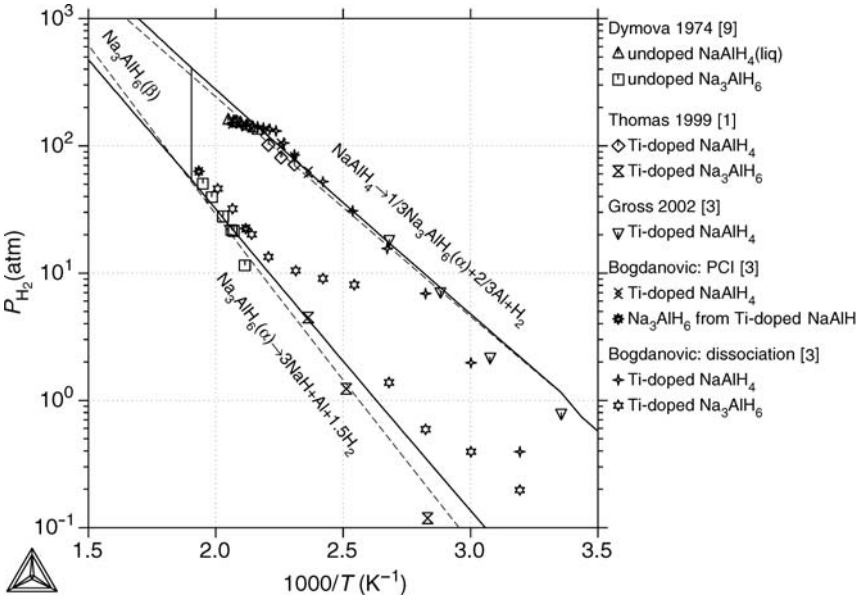

Fig. 6. Calculated dissociation pressure of $NaAlH_4$ and Na_3AlH_6 as a function of temperature in comparison with experimental data. The dashed lines represent the phonon direct method predictions.

From the above discussion it is seen that the dissociation enthalpy ΔH for each hydride is related to the slope of the corresponding line in Fig. 6. To examine the effect of temperature, the dissociation enthalpy and entropy were calculated for $NaAlH_4$ and α-Na_3AlH_6 as a function of temperature in Fig. 7a and b, where the dissociation enthalpy for NaH is also plotted for comparison. From Fig. 7a and b it is clear that the dissociation enthalpy and entropy exhibit very weak temperature dependence. As a consequence, it is expected that there will be an approximate linear dependence of the dissociation Gibbs energy on temperature. This is also true for the Gibbs energy of formation of $NaAlH_4$, α-Na_3AlH_6, and β-Na_3AlH_6 shown in Fig. 8, where the curve for α-Na_3AlH_6 almost coincides with that for β-Na_3AlH_6. There are no direct experimental data to show temperature dependence of the Gibbs energy. Fortunately, such temperature dependence has been predicted by the Phonon direct method calculations, as shown by symbols in Fig. 8. It is seen that the present thermodynamic modeling has almost the same temperature dependence as the Phonon direct method predictions, although there was a small difference for $NaAlH_4$ and α-Na_3AlH_6. The difference was a consequence of the fact that the thermodynamic modeling was weighted to rely more heavily on experimental data, rather than the data from the Phonon direct method predictions. This can also be seen from Table 4, in which the standard enthalpy of formation of $NaAlH_4$ and α-Na_3AlH_6 are listed according to the present thermodynamic modeling and Phonon direct method predictions, in comparison with data from literature. Data for

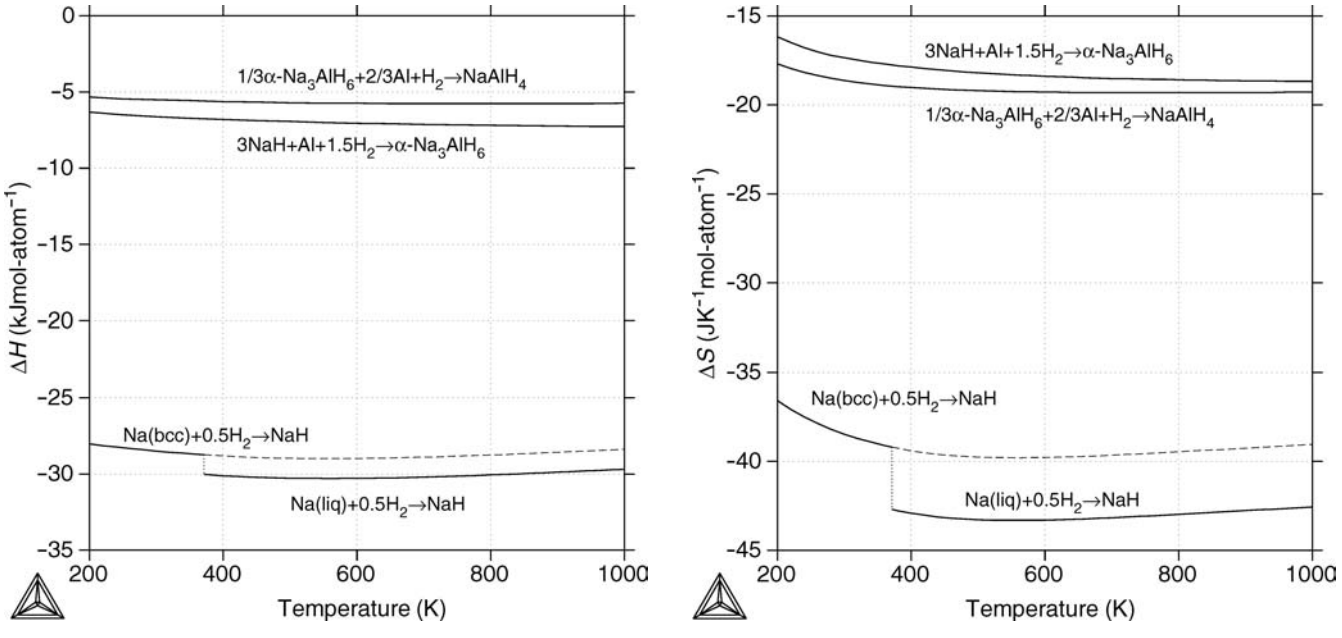

(a) (b)

Fig. 7. Calculated (a) dissociation enthalpy and (b) dissociation entropy according to the dissociation reactions for $NaAlH_4$, α-Na_3AlH_6, and NaH at various temperatures.

NaH are also given in Table 4, which were discussed in Reference [26].

By combining the three binary Al–Na, Al–H, and Na–H systems with thermodynamic descriptions of $NaAlH_4$, α-Na_3AlH_6, and β-Na_3AlH_6, ternary diagrams can be calculated under various conditions. As an example, isothermal sections of the Na–Al–H system were calculated at 100 °C at 1 atm and 100 atm, respectively, to show phase relations in Fig. 9a and b. It is seen that $NaAlH_4$ was not stable at 1 atm, but it becomes stable at 100 atm. Vertical sections calculated along the composition line NaH–AlH_3 at 1 atm and 100 atm are presented in Fig. 10a and b to show stability of hydrides and their decomposition reactions.

A potential diagram of the ternary system is presented in Fig. 11 to show stability of each phase and the relations among the various phases. Each single phase area in Fig. 11 represents the temperature and hydrogen activity ranges for stable phase existence. A line stands for an equilibrium between two phases with or without fcc Al, and a cross-point of three lines is for the three-phase equilibrium with or without fcc Al. It is noted from Fig. 11 that $NaAlH_4$ and NaH are separated by α-Na_3AlH_6, indicating a two-step decomposition of $NaAlH_4$, as observed in experiments [6]. To demonstrate the effect of hydrogen pressure on the formation of various hydrides at a given temperature, a diagram of the Al–Na system was calculated at 100 °C, as shown in Fig. 12. It can be seen that at 100 °C $NaAlH_4$ decomposes into α-Na_3AlH_6 and fcc Al at 17 atm, while α-Na_3AlH_6 decomposes into NaH and fcc Al at 0.76 atm. The melting of α-Na_3AlH_6 at 20 807 atm and melting of $NaAlH_4$ at 1.345×10^6 atm predicted at 100 °C has not been validated by experiments.

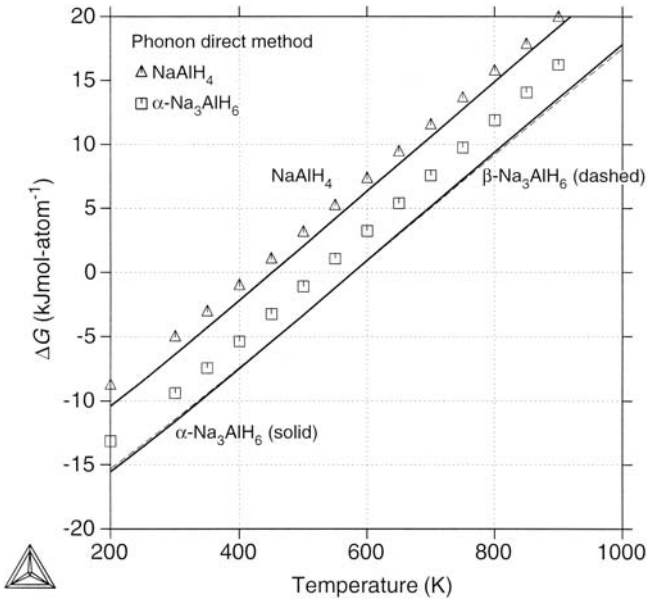

Fig. 8. Calculated Gibbs energy of formation of $NaAlH_4$, α-Na_3AlH_6, and β-Na_3AlH_6 as a function of temperature, in comparison with the predictions from the Phonon direct methods.

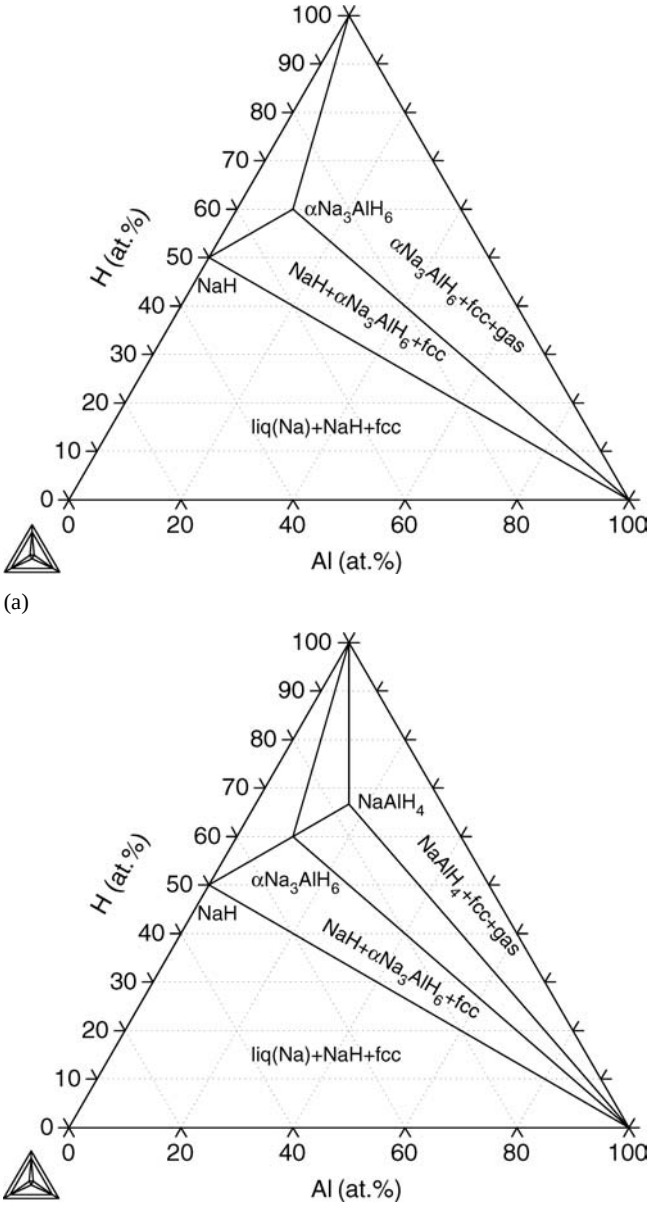

Fig. 9. Isothermal sections of the Na–Al–H system calculated at 100 °C at (a) 1 atm and (b) 100 atm.

Table 4. The standard enthalpy of formation [kJ (mole atom)$^{-1}$] of NaH, $NaAlH_4$, and α-Na_3AlH_6, at 298.15 K and 1bar according to the present thermodynamic modeling and Phonon direct method predictions in comparison with experimental data from literature. Data for NaH were discussed in Reference [26].

NaH	$NaAlH_4$	α-Na_3AlH_6	β-Na_3AlH_6	Remark
−28 ~ −29	−18.83 ~ −19.50	–	–	Experiment [7–8]
−28.49	−18.67	−23.71	−23.36	Thermodynamic modeling [this work]
−24.30	−17.48	−22.48	–	Phonon direct method prediction [this work]

5. Conclusions

The first-principles methodology linking density functional theory ground state minimizations with direct method lattice dynamics was applied to predict the finite temperature thermodynamic properties of the $NaAlH_4$, α-Na_3AlH_6, and β-Na_3AlH_6 phases. It has been shown that the predictions of heat capacity and dissociation pressures for $NaAlH_4$ and α-Na_3AlH_6 were in satisfactory agreement with experimental data, which can be taken as an indication that the theoretical approach was well justified.

Based on experimental data and first-principles predictions, the stability of sodium alanates was assessed using thermodynamic models. The model calculations show very good agreement with experimental data, including the enthalpy of decomposition from the dissociation pressure of the sodium alanates, and their stability under various conditions. These results demonstrate the utility of combining first-principles predicted and experimentally measured thermodynamic data to improve both the physical basis and the reliability of CALPHAD thermodynamic assessments. This integrated experimental–theoretical approach allows for the validation of first-principles data and the extension of thermodynamic predictions beyond the experimental realm.

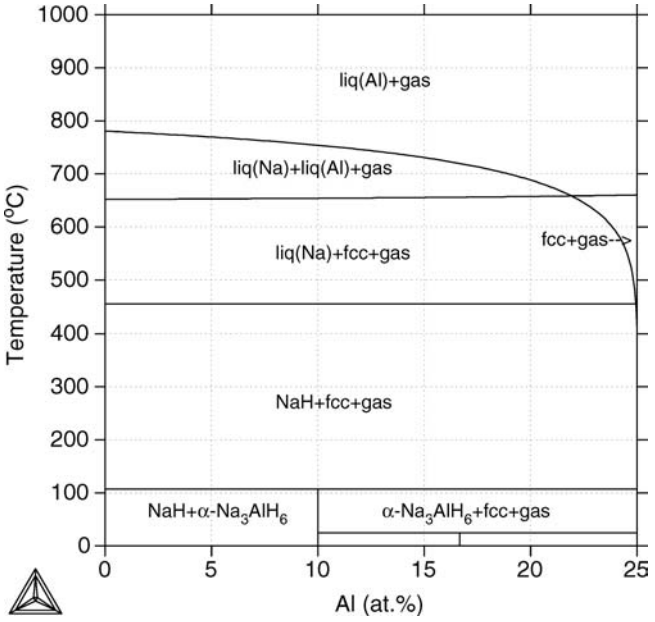

(a)

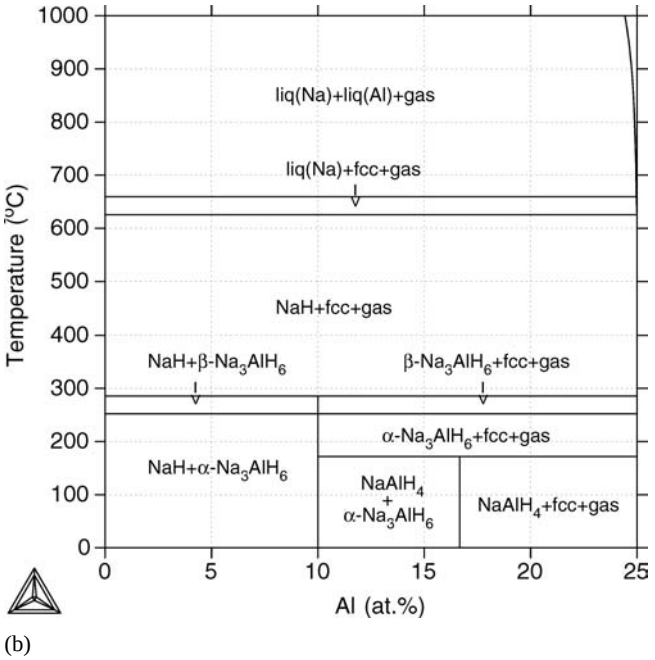

(b)

Fig. 10. Vertical sections of the Na–Al–H system calculated along the composition line $NaH–AlH_3$ at (a) 1 atm and (b) 100 atm.

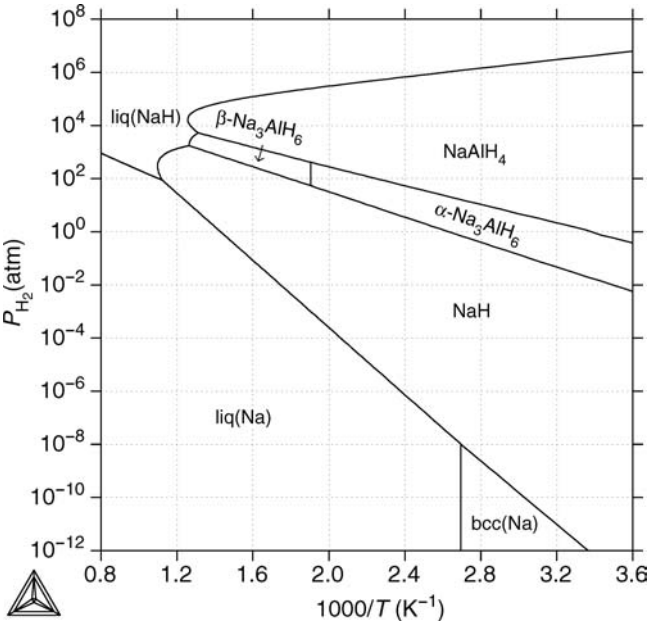

Fig. 11. Calculated potential diagram of the Na–Al–H system to show the stability of various phases and their relationship.

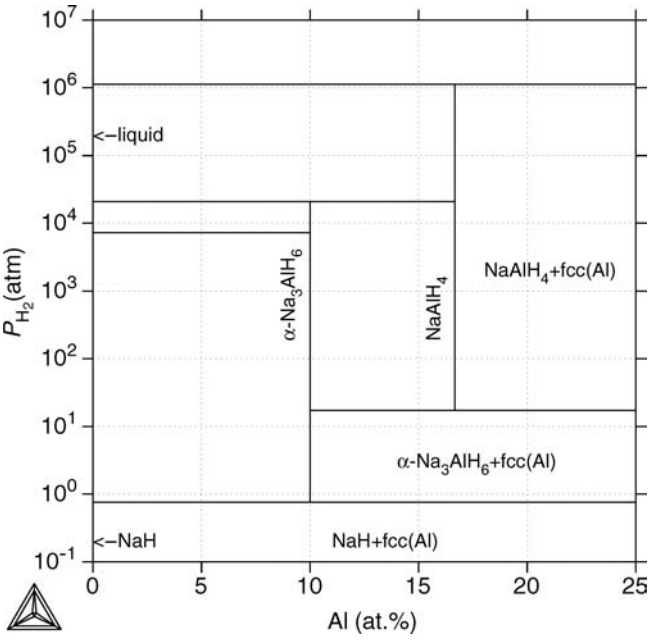

Fig. 12. Effect of hydrogen pressure on the formation of various hydrides at 100 °C according to the present calculation.

This work was financially supported by the United States Department of Energy under contract DE-FC04-02AL67610, managed by United Technologies Research Center, East Hartford, Connecticut, USA. S. M. Opalka gratefully acknowledges valuable discussions with Paul Saxe of Materials Design, Inc., Taos, New Mexico, USA.

References

[1] G.J. Thomas, S.E. Gunthrie, K. Gross: Proceedings of the US DOE Hydrogen Program Review, NREL/CP-570-26938, San Ramon, CA, USA (1999).
[2] B. Bogdanovic, R.A. Brand, A. Marjanovic, M. Schwickardi, J. Tolle: J. Alloys Comp. 302 (2000) 36.
[3] K.J. Gross, G.J. Thomas, C.M. Jensen: J. Alloys Comp. 330–332 (2002) 683.
[4] P. Claudy, B. Bonnetot, J.M. Letoffe, G. Turck: Thermochimica Acta 27 (1978) 199.
[5] P. Claudy, B. Bonnetot, G. Chahine, J.M. Letoffe: Thermochimica Acta 38 (1980) 75.
[6] B. Bonnetot, G. Chahine, P. Claudy, M. Dior, J.M. Letoffe: J. Chem. Thermodynamics 12 (1980) 249.
[7] M.B. Smith, G.E. Brass: J. Chem. Eng. Data 8 (1963) 342.
[8] P. Claudy, J.M. Letoffe, G. Chahine, B. Bonnetot: Thermochimica Acta 78 (1984) 323.
[9] T.N. Dymova, Y.M. Dergachev, V.A. Sokolov, N.A. Grechanaya: Doklady Akademii Nauk SSSR 224 (1975) 556.
[10] B. Yebka, G.-A. Nazri: Mat. Res. Soc. Symp. Proc. 801 (2004) 133.
[11] C. Batzner, S. Gama, in: Ternary Alloys, Vol. 6, VCH Verlagsgesellschaft, Weinheim, FGR (1993) 118.
[12] S.M. Opalka, D.L. Anton: J. Alloys Comp. 356–357 (2003) 486.
[13] C. Wolverton, V. Ozolins, M. Asta: Phys. Rev. B 69 (2004) 144109-1.
[14] M.E. Arroyo y de Dompablo, G. Ceder: J. Alloys Comp. 364 (2004) 6.
[15] X. Ke, I. Tanaka: Phys. Rev. B 71 (2005) 024117.
[16] V. Ozolins, E.H. Majzoub, T.J. Udovic: J. Alloys Comp. 375 (2004) 1.
[17] J. Iniguez, T. Yildirim, T.J. Udovic, M. Sulic, C.M. Jensen: Phys. Rev. B 70 (2004) 060101.
[18] A. Peles, J.A. Alford, Z. Ma, L. Yang, M.Y. Chou: Phys. Rev. B 70 (2004) 165105.
[19] C.M. Araujo, S. Li, R. Ahuja, P. Jena: Phys. Rev. B 72 (2005) 165101.
[20] G. Kresse, J. Hafner: Phys. Rev. B 47(1) (1993) 558.
[21] G. Kresse, J. Furthmuller: Comput. Mater. Sci. 6 (1996) 15.
[22] G. Kresse, J. Furthmuller: Phys. Rev. B 54(16) (1996) 11169.
[23] K. Parlinski, Z.Q. Li, Y. Kawazoe: Phys. Rev. Lett. 78 (1997) 4063.
[24] MedeA-Phonon Version 1.0 using Phonon Software 3.11, Copyright K. Parlinski.
[25] C. Qiu, G.B. Olson, S.M. Opalka, D.L. Anton: J. Phase Equilibria Diff. 25 (2004) 520.
[26] C. Qiu, S.M. Opalka, G.B. Olson, D.L. Anton: Int. J. Mat. Res. (formerly Z. Metallkd.) 97 (2006) 845.
[27] J.L. Murray: Bull. Alloy Phase Diagrams 4 (1983) 407.
[28] W.L. Fink, L.A. Willey, H.C. Stumpf: Trans. AIME 175 (1948) 364.
[29] C.E. Ransley, H. Neufeld: J. Japn. Inst. Met. 78 (1950) 25.
[30] E. Scheuber: Z. Metallkd. 27 (1933) 83.
[31] S.G. Hansen, J.K. Tuset, G.M. Haarberg: Metall. Trans. B 33 (2002) 577.
[32] E.W. Dewing: Metall. Trans. 1 (1970) 1691.
[33] R.J. Brisley, D.J. Fray: Metall. Trans. B 14 (1983) 435.
[34] B. Bogdanovic, G. Sandrock: Mat. Res. Soc. Bull. 27 (2002) 712.
[35] J.P. Perdew, J.A. Chevary, S.H. Vosko, K.A. Jackson, M.R. Pederson, D.J. Singh, C. Fiolhais: Phys. Rev. B 46 (11–15) (1992) 6671.
[36] G. Kresse, D. Joubert: Phys. Rev. B 59(3) (1999) 1758.
[37] H.J. Monkhorst, J.D. Pack: Phys. Rev. B 13 (1976) 5188.
[38] I. Ansara, B. Sundman, in: P.S. Glaeser (Ed.), Computer Handling and Dissemination of Data, Vol. 1, North-Holland, Amsterdam (1987) 154.
[39] M.W. Chase, Jr.: NIST-JANAF Themochemical Tables, 4th Ed., J. Phys. Chem. Ref. Data, Monograph 9 (1998) 1.
[40] M. Hillert: Phase Equilibria, Phase Diagrams and Phase Transformations, Cambridge University Press, Cambridge (1998) 428.
[41] J. Agren, B. Cheynet, M.T. Clavaguera-Mora, J. Hertz, K. Hack, F. Sommer, U. Kattner: CALPHAD 19 (1995) 449.
[42] Thermo-Calc software, AB.
[43] H.E. Swanson, E. Tatge: Nat. Bur. Stand. U.S. Circ. 539 359 (1953) 1.
[44] K.J. Gross, S. Guthrie, S. Takara, G. Thomas: J. Alloys Comp. 297 (2000) 270.
[45] B.C. Hauback, H.W. Brinks, C.M. Jensen, K. Murphy, A.J. Maeland: J. Alloys Comp. 358 (2003) 142.
[46] E. Ronnebro, D. Noreus, K. Kadir, A. Reiser, B. Bogdanovic: J. Alloys Comp. 299 (2000) 101.
[47] P. Vajeeston, P. Ravindran, R. Vidya, H. Fjellvag, A. Kjekshus: Appl. Phys. Lett. 82 (2003) 2257.
[48] A. Aguayo, D.J. Singh: J. Phys. Rev B 69 (2004) 155103.
[49] S.-C. Chung, H. Morioka: J. Alloys Comp. 372 (2004) 92.
[50] T.J. Frankcombe, O.M. Lovvik: J. Phys. Chem. B 110 (2006) 622.
[51] A.T. Dinsdale, CALPHAD 15 (1991) 317.

(Received January 30, 2006; accepted July 10, 2006)

Correspondence address

Susanne M. Opalka, Ph. D.
United Technologies Research Center,
411 Silver Lane, MS 129-22
East Hartford, CT, USA 06108
Tel.: +1 860 610 7195
E-mail: opalkasm@utrc.utc.com

You will find the article and additional material by entering the document number MK101410 on our website at www.ijmr.de

Appendix

Summary of thermodynamic parameters describing the Na–Al–H system. Values are given in SI units (Joule, mole, Kelvin, and Pa) and correspond to one mole of formula units of the phases. The parameters marked with an asterisk (*) were evaluated in the present work. Gibbs energy for gas and pure elements can be found in References [39] and [51], respectively.

Liquid with formula (Al, H, Na)

$${}^{o}G_{H}^{liq} = 8035 + 25T + 2T\ln(T) + 0.5\times F10784T$$

$$L_{Al,H}^{liq} = 50\,942 - 11.1007T$$

$$L_{Al,Na}^{liq} = 14\,130 + 56.0985T - 1827\times(x_{Al} - x_{Na}) \qquad (*)$$

$$L_{H,Na}^{liq} = -70\,264 + 45.2458T + (-56\,577 + 21.8825T) \times (x_{H} - x_{Na})$$

BCC_A2 with formula $(Al, Na)_1(H, Na)_3$

$${}^{o}G^{bcc}_{Al:H} = 200\,000 + {}^{o}G^{AlH3}_{Al:H}$$

$${}^{o}G^{bcc}_{Na:H} = 215\,965 + 3RT\ln[\exp(0.5\times 215/T) - \exp(-0.5\times 215/T)] - 0.0095113T^2$$

for 0 K < T < 298.15 K

$$= 206\,754 + 258.2187T - 42.90288T\ln T - 0.004047T^2 + 1.889\times 10^{-7}T^3 + 696\,986/T$$

for 298.15 K < T < 2000 K

$$L^{bcc}_{Al,Na:Va} = 27\,715 \quad (*)$$

FCC_A1 with formula $(Al, Na)_1(H, Va)_1$

$${}^{o}G^{fcc}_{Al:H} = 100\,000 + {}^{o}G^{fcc}_{Al} + 0.5{}^{o}G^{gas}_{H2}$$

$${}^{o}G^{fcc}_{Na:H} = 130T + {}^{o}G^{bcc}_{Na} + 0.5{}^{o}G^{gas}_{H2}$$

$$L^{fcc}_{Al:H,Va} = -45\,805 + 56.4302T$$

$$L^{fcc}_{Al,Na:Va} = -6210 + 76.4864T \quad (*)$$

AlH_3 with formula $(Al)_1(H)_3$

$${}^{o}G^{AlH3}_{Al:H} = -28\,415 + 213.712933T - 41.75632T\ln(T) - 0.014548469T^2 + 446\,400/T$$

NaH with formula $(Na)_1(H)_1$

$${}^{o}G^{NaH}_{Na:H} = -66\,593 + 3RT\ln[\exp(0.5\times 268/T) - \exp(-0.5\times 268/T)] - 0.0188755T^2$$

for 0 K < T < 298.15 K

$$= -75\,768 + 293.7188T - 48.6935T\ln T - 2.614\times 10^{-4}T^2 + 1.8048\times 10^{-8}T^3 + 632\,658/T$$

for 298.15 K < T < 2000 K

$NaAlH_4$ with formula $(Na)_1(Al)_1(H)_4$

$${}^{o}G^{NaAlH4}_{Na:Al:H} = -128\,890 - 0.10258T^2 + 3RT\ln[\exp(0.5\times 220/T) - \exp(-0.5\times 220/T)]$$

for 0 K < T < 298.15 K (*)

$$= -150\,434 + 592.2826T - 99.0677T\ln T - 0.018466T^2 + 1.0858\times 10^{-6}T^3 + 1\,091\,420/T$$

for 298.15 K < T < 2000 K (*)

α-Na_3AlH_6 with formula $(Na)_3(Al)_1(H)_6$

$${}^{o}G^{\alpha-Na3AlH6}_{Na:Al:H} = -267\,960 - 0.17245T^2 + 6RT\ln[\exp(0.5\times 217/T) - \exp(-0.5217/T)]$$

for 0 K < T < 298.15 K (*)

$$= -309\,621 + 1122.177T - 187.24T\ln T - 0.0226T^2 + 1.3138\times 10^{-6}T^3 + 2\,200\,845/T$$

for 298.15 K < T < 2000 K (*)

β-Na_3AlH_6 with formula $(Na)_3(Al)_1(H)_6$

$${}^{o}G^{\beta-Na3AlH6}_{Na:Al:H} = 3497 - 6.6587T + {}^{o}G^{\alpha-Na3AlH6}_{Na:Al:H} \quad (*)$$